

# JigsawComm: Joint Semantic Feature Encoding and Transmission for Communication-Efficient Cooperative Perception

Chenyi Wang<sup>1</sup>, Zhaowei Li<sup>2</sup>, Ming F. Li<sup>1</sup>, and Wujie Wen<sup>2</sup>

<sup>1</sup> University of Arizona, Tucson AZ 85719, USA

<sup>2</sup> North Carolina State University, Raleigh NC 27695, USA  
 {chenyiw,lim}@arizona.edu {zli223,wwen2}@ncsu.edu

**Abstract.** Multi-agent cooperative perception (CP) promises to overcome the inherent occlusion and range limitations of single-agent systems in autonomous driving, yet its practicality is severely constrained by limited Vehicle-to-Everything (V2X) communication bandwidth. Existing approaches attempt to improve bandwidth efficiency via compression or heuristic message selection, but neglect the semantic relevance and cross-agent redundancy of the transmitted data. In this paper, we formulate a joint semantic feature encoding and transmission problem that maximizes CP accuracy under a communication budget, and introduce JIGSAWCOMM, an end-to-end semantic-aware framework that learns to “assemble the puzzle” of multi-agent feature transmission. JIGSAWCOMM uses a regularized encoder to extract *sparse, semantically relevant features*, and a lightweight Feature Utility Estimator (FUE) to predict each agent’s per-cell contribution to the downstream perception task. The FUE-generated compact meta utility maps are exchanged among agents and used to compute an optimal transmission policy under the learned utility proxy. This policy inherently *eliminates cross-agent redundancy*, bounding the feature transmission payload to  $\mathcal{O}(1)$  as the number of agents grows, while the meta information overhead remains negligible. The whole pipeline is trained end-to-end through a differentiable scheduling module, informing the FUE to be aligned with the task objective. On the OPV2V and DAIR-V2X benchmarks, JIGSAWCOMM reduces total data volume by over 20–500× while matching or exceeding the accuracy of state-of-the-art methods.

## 1 Introduction

Multi-agent cooperative perception (CP) enables connected road agents, such as connected and autonomous vehicles (CAVs) and road-side units (RSUs), to improve their understanding of the environment [14]. By leveraging sensor data exchanged through Vehicle-to-Everything (V2X) communication [7], participating agents can detect objects beyond their individual sensing ranges, minimize blind spots, and perceive occluded obstacles [36]. With its great potential for facilitating more informed driving decisions and enhancing road safety, CP is a critical technology for 50–90% of the vehicle market that CAVs are anticipated to comprise by 2040 [2].

Despite this promise, CP faces a formidable challenge in communication efficiency. The available V2X bandwidth is severely limited (up to 20 MHz for both DSRC [9]



**Fig. 1:** A sample scenario from the OPV2V dataset (left). Under the same bandwidth limit, prior work [10] (middle) does not utilize bandwidth efficiently, leading to missed detections. JIGSAW-COMM (right) maximizes every bit’s contribution, enabling complete and accurate detection. See Sec. 4 for quantitative evaluation and discussion on the “cost” of redundancy.

and C-V2X [8]), while the volume of sensor data generated is prohibitively large (e.g. 4 MB per LiDAR frame [3]). Exchanging raw sensor data is therefore infeasible while satisfying the stringent real-time perception requirements of autonomous driving (e.g.  $<100$  ms [17]). As previous research also demonstrated that exchanging local detection results alone is suboptimal [36], the field has largely converged on the intermediate fusion framework—exchanging and fusing Bird’s-Eye-View (BEV) features—as the most effective paradigm [3, 10, 35, 36]. Even so, transmitting dense deep features from multiple agents still exhausts V2X bandwidth.

The key challenge stems from the high degree of data redundancy in the shared features, which takes two forms: (i) *intra-agent* redundancy, where features waste bits on semantically irrelevant information; and (ii) *inter-agent* redundancy, where multiple agents transmit overlapping data about the same scene regions. As illustrated in Fig. 1, under limited bandwidth such inefficiency not only reduces detection coverage but can even degrade perception accuracy when lower-quality data dilutes higher-quality representations after fusion (Sec. 4.4).

Existing communication-efficient CP methods fail to address both forms simultaneously. They typically adopt one of two strategies: (i) *Compression*, using encoder-decoders [36] or codebooks [11, 43], which reduce data size but still transmit the entire feature map or restrict representation power to offline-trained dictionaries; (ii) *Message selection* [10, 11, 19, 33], choosing “critical” regions based on local heuristics (e.g. detection confidence) that loosely correlate with the final cooperative task. Crucially, both approaches ignore cross-agent redundancy, so their communication cost still grows linearly with the number of agents. *The problem of designing a truly communication-efficient, scalable, and accurate CP system remains open.*

We argue that a practical CP system must maximize the contribution of every transmitted bit to the final perception goal, transmitting only essential, semantically meaningful, and non-redundant information. This requires *jointly* designing the feature encoding and transmission selection, which is non-trivial: removing cross-agent redundancy is a “chicken-and-egg” problem, since an agent cannot determine whether its features are redundant without knowing what other agents intend to transmit.

To address these gaps, we propose JIGSAW-COMM, an end-to-end semantic-aware CP framework that learns to “assemble the puzzle” of multi-agent feature transmission. First, a regularized feature encoder extracts features that are both semantically important and sparse. Second, a lightweight Feature Utility Estimator (FUE) predicts each agent’s per-cell contribution to the final perception result, producing compact *meta utility maps* that approximate the marginal value of each feature and expose cross-agent overlap.

The entire framework is trained end-to-end via a differentiable scheduler that jointly optimizes the encoder and FUE. At inference, agents exchange meta utility maps and locally compute an explainable, deterministic transmission policy: select at most one agent with the highest utility per cell, then greedily admit cells until the communication budget is met. We prove this policy is optimal under the learned utility proxy (Theorems 1 and 2) and validate its alignment with task accuracy empirically.

The top-1-per-cell rule inherently eliminates cross-agent duplication by construction, making the system practical and scalable: the final transmission is a sparse “jigsaw” assembled from the best cell-level features across agents, bounding the data-channel cost to  $\mathcal{O}(1)$  with respect to the number of agents  $N$ , compared to  $\mathcal{O}(N)$  for naive broadcast. Although exchanging the lightweight meta utility maps incurs  $\mathcal{O}(N)$  signaling, this overhead is negligible in practice ( $<0.03$  KB per frame). The scheduler yields identical decisions on every agent, making it deployable in both centralized (V2I) and decentralized (V2V) modes. Our contributions are:

- We propose JIGSAWCOMM, a CP framework that jointly trains a sparse semantic encoder and an end-to-end differentiable scheduler to maximize each transmitted bit’s contribution to perception accuracy.
- We introduce a learned, task-aligned utility proxy and a top-1-per-cell scheduling policy that eliminates cross-agent redundancy and bounds data-channel cost to  $\mathcal{O}(1)$  with respect to the number of agents.
- We extensively evaluate JIGSAWCOMM on the OPV2V [36] and DAIR-V2X [37] benchmarks, demonstrating SOTA accuracy and 20–500 $\times$  bandwidth reduction compared with prior art (*e.g.* Where2comm, NIPS’22 [10]; ERMVP, CVPR’24 [40]; CoST, ICCV’25 [30]).<sup>3</sup>
- Our results uncover a counterintuitive ‘more is worse’ effect in existing CP fusion backbones, showing that redundant multi-agent features can *degrade* accuracy rather than improve it. We highlight the need for future CP fusion architectures that can effectively leverage, instead of suffer from, redundancy.

## 2 Background and Related Work

### 2.1 Cooperative Perception Paradigms

Research in CP has explored various strategies for fusing information from multiple agents, which are primarily categorized by the stage at which fusion occurs. Early fusion involves the transmission and aggregation of raw sensor data, such as LiDAR point clouds or camera images [41, 42]. While this approach theoretically preserves the maximum amount of information, it is prohibitively expensive in terms of required communication bandwidth and is thus considered impractical for real-world V2X applications [3]. At the other extreme, late fusion operates on the final perception outputs, where agents directly exchange local perception results [26]. This method is highly communication-efficient but suffers from significant information loss during local processing, making it difficult to resolve detection conflicts and susceptible to error propagation [36].

<sup>3</sup> Code available at <https://github.com/WiSeR-Lab/JigsawComm>.

The dominant paradigm in modern CP is intermediate fusion, which strikes a balance between these two extremes [3, 10, 19, 33, 35, 36]. In this approach, agents first process their raw sensor data into an intermediate feature representation, typically within a shared and aligned BEV grid. These features are then exchanged and fused before being passed to a final detection head. This strategy preserves rich semantic and spatial information while being more communication-friendly than early fusion, forming the basis for most state-of-the-art methods, including JIGSAWCOMM proposed in this paper.

## 2.2 Communication-Efficient CP Strategies

Within the intermediate fusion paradigm, several previous works have focused on optimizing the trade-off between perception performance and communication cost. These efforts can be broadly classified by their core strategy.

**Message Representation.** This category compresses feature maps via encoder-decoders [33, 36, 40], codebook quantization [11, 43], or generative reconstruction [21, 40, 44]. Encoder-decoder approaches apply a bottleneck to reduce the feature dimensionality, achieving fixed compression ratios but lacking adaptability to varying scene complexity. Codebooks approximate continuous features with discrete indices matching to an offline trained dictionary, which may restrict the generalizability of the representation [11, 43]. Diffusion-based methods achieve high accuracy-bandwidth tradeoff (*e.g.* 0.86 mAP@0.5 under 80 Kbps [21]) but the multi-step denoising violate real-time computation latency constraints for autonomous driving [17]. Crucially, these approaches compress the *entire* feature map uniformly without considering which regions are task-relevant, wasting bits on uninformative background.

**Message Selection.** This line of research aims to prune the information sent by agents, assuming that not all data is equally valuable. Early work like When2com [19] employed a GNN to select which agents to communicate with, performing a coarse, agent-level selection. However, as V2X communication primarily relies on wireless broadcast rather than direct pairwise communications [8, 9], optimizing communication graphs does not save bandwidth in practice. A more fine-grained approach was introduced by Where2comm [10], which has become the *de facto* canonical baseline for communication-efficient CP, which generate a spatial confidence map by applying the *detector head* on each agent’s local feature. This map serves as a heuristic to identify ‘perceptually critical’ regions for transmission, which achieves region-level sparsity, reducing bandwidth compared to sending dense feature maps. Follow-up work extends this idea with spatiotemporal fusion [30] or intermediate-late hybrid fusion [33]. However, these methods rely on local detection confidence that may not correlate well with the final CP accuracy and lack mechanisms to suppress inter-agent redundancy, resulting in  $\mathcal{O}(N)$  communication scaling. Prior attempts at redundancy reduction either use geometry-based heuristics that ignore semantics [25, 31, 38, 42] or mutual information metrics that are computationally impractical [29, 32].

**Positioning Our Work.** Existing communication-efficient CP methods share three unresolved shortcomings: reliance on heuristic utility proxies; no explicit modeling of semantic inter-agent redundancy; and static performance-bandwidth trade-offs. Our work addresses all three by introducing a semantic-aware, task-oriented, end-to-end learned

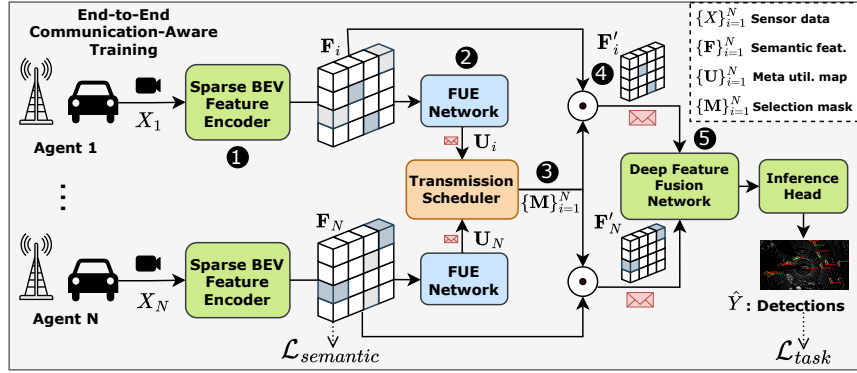


**Fig. 2:** Overview of JIGSAWCOMM. Each agent encodes sparse BEV features, estimates a meta utility map via the FUE, exchanges utility maps, and applies the deterministic top-1-per-cell scheduler to select non-redundant features for transmission and fusion.

scheduling policy that is adaptive to varying bandwidth. While JIGSAWCOMM shares the high-level goal of task-oriented compression with semantic/goal-oriented communications [23, 28], existing work in that field targets single-source scenarios [1, 39] or neglects inter-sensor correlations [27]. CP is inherently a *multi-source* problem where inter-agent redundancy must be modeled without knowing the data correlation structure *a priori*; JIGSAWCOMM solves this in a data-driven manner, with minimal overhead.

### 3 Methodology

#### 3.1 Problem Formulation

We consider  $N$  agents  $\mathcal{A} = \{a_1, \dots, a_N\}$  collaborating via V2X<sup>4</sup>. Per cycle, agent  $a_i$  obtains raw sensor data  $X_i$  and uses an encoder  $\Phi_{enc}$  to produce a BEV feature map  $F_i = \Phi_{enc}(X_i) \in \mathbb{R}^{C \times H \times W}$  with cells  $f_l^i \in \mathbb{R}^C$ ,  $l \in \mathcal{L} = \{1, \dots, L\}$ ,  $L=HW$ . After exchanging meta utility maps  $\mathbf{U}_{i=1}^N$ , each agent  $a_i$  then transmits a sparse subset  $F'_i = \mathbf{M}_i \odot F_i$ , where  $\mathbf{M}_i \in \{0, 1\}^{H \times W}$  and  $\odot$  denotes element-wise multiplication. A fusion module  $\Phi_{fuse}$  and decoder  $\Phi_{dec}$  produce the output  $\hat{Y}$ . Our goal is to maximize the CP accuracy within a total communication budget  $B^5$ :

$$\max_{\theta, \{\mathbf{M}_i\}_{i=1}^N} \mathcal{P}(\Phi_{dec}(\Phi_{fuse}(\{\mathbf{M}_i \odot \Phi_{enc}(X_i)\}_{i=1}^N)), Y) \quad (1)$$

$$\text{s.t.} \quad \sum_{i=1}^N |\mathbf{M}_i \odot \Phi_{enc}(X_i)| \leq B. \quad (2)$$

Here,  $\mathcal{P}(\cdot)$  is the CP accuracy evaluation metric (*e.g.* mAP),  $Y$  corresponds to the ground truth supervision,  $\theta$  denotes the trainable parameters for the entire network, and the binary masks  $\{\mathbf{M}_i\}_{i=1}^N$  select subsets of the encoded features across spatial

<sup>4</sup> Here, agents can be CAVs or RSUs, within the same V2X communication range.

<sup>5</sup>  $B$  equals the available bandwidth  $BW$  divided by the frame rate  $r$ .

dimensions for transmission and fusion. During training, Eq. (1) is optimized jointly over the model parameters  $\theta$  and the transmission masks  $\{\mathbf{M}_i\}$  via the differentiable scheduler (Sec. 3.4); at inference,  $\theta$  is fixed and only the scheduling masks  $\{\mathbf{M}_i\}$  are optimized.

**Challenges.** This formulation presents three core challenges: (C1) During inference, each agent must decide *which* features to transmit without access to ground truth or full features from other agents (infeasible to transmit) to optimize for  $\mathcal{P}(\cdot)$ . Thus, a locally computable and compact utility proxy that correlates with CP accuracy and captures cross-agent redundancy is required. (C2) The binary scheduling masks  $\mathbf{M}_i$  are non-differentiable, preventing direct end-to-end training of the utility proxy. (C3) The feature selection under Eq. (2) is a 0-1 knapsack problem, which is NP-Hard in general [13].

**System Overview.** JIGSAWCOMM learns to assemble the ‘jigsaw’ of multi-agent BEV features so that the CP messages carry only essential, non-overlapping content. As shown in Fig. 2, *each agent*: ❶ produces *sparse and semantically important* features (Sec. 3.2); ❷ predicts a compact meta utility map using a Feature Utility Estimator (FUE) network, which is exchanged among agents efficiently (Sec. 3.3); ❸ locally applies a *deterministic, redundancy-aware* top-1-per-cell policy, producing a feature selection mask that maximizes the total utility while satisfying the communication budget (Sec. 3.4); ❹ broadcasts the selected features; ❺ fuses the exchanged features and passes to the inference head for output. With the total per-frame data payload upper-bounded by the size of a single sparse semantic feature, the data-channel bandwidth scales as  $\mathcal{O}(1)$  with respect to the number of agents, ensuring high scalability.

### 3.2 Sparse Semantic Feature Encoder

To ensure that features carry compact and *essential* semantics using a minimal number of bits, we first shape the encoder’s output to reduce intra-agent redundancy. We apply a semantic loss consisting of an  $L_1$  regularization and a learnable threshold  $\kappa$  on the encoded feature  $\mathbf{f}_i$ :

$$\mathcal{L}_{\text{semantic}} = \frac{1}{NL} \sum_{i=1}^N \sum_{l=1}^L \|\mathbf{f}_i^l \odot \mathbb{I}\{\mathbf{f}_i^l > \kappa\}\|_1. \quad (3)$$

$L_1$  regularization is known to produce sparse coefficients and suppress irrelevant features [22]. However, applying it directly to raw activations ( $\|\mathbf{f}_i^l\|_1$ ) only encourages small magnitudes without yielding *exact zeros*—uninformative activations linger at small but nonzero values, still consuming bits. The learnable threshold  $\kappa$  resolves this by explicitly zeroing out activations below  $\kappa$ , producing structurally sparse features with exact zeros that incur no transmission cost under sparse index encoding [10].

### 3.3 Feature Utility Estimator (FUE)

**Utility Proxy.** As established in task-oriented and semantic communication [24, 28], higher CP accuracy correlates with transmitted data retaining more information about the final inference result. Therefore, to address (C1), we design a utility function  $U(\cdot)$  that serves as a proxy for the downstream CP accuracy and can be computed locally

from the agents’ features.  $U$  aggregates the individual feature contributions of all agents and penalizes pairwise redundancy. The utility at each spatial cell  $l$  is defined as:

$$U^l = \underbrace{\sum_{i=1}^N m_i^l u_i^l}_{\text{importance}} - \underbrace{\sum_{j \neq i} \frac{m_i^l m_j^l \tilde{u}_{ij}^l}{2}}_{\text{overlap penalty}}, \tilde{u}_{ij}^l \triangleq \min\{u_i^l, u_j^l\}. \quad (4)$$

Here,  $m_i^l \in \{0, 1\}$  is the binary transmission decision for  $\mathbf{f}_i^l$  and  $u_i^l$  is its estimated importance—the FUE predicted contribution of agent  $i$ ’s feature at cell  $l$  to the CP result. The term  $\tilde{u}_{ij}^l$  conservatively upper-bounds the pairwise redundancy between agents  $i$  and  $j$ , with the  $\frac{1}{2}$  factor avoiding double-counting [4]. Since features in the same BEV cell describe the same physical location; overlapping observations typically differ only in strength, making  $\min(\cdot)$  a tractable upper bound on shared information. The frame-level utility is  $U = \sum_{l=1}^L U^l$ , which serves as a first-order approximation of task-relevant information by rewarding informative features and penalizing redundancy [4].

**Scope of the Utility Proxy.** We emphasize that  $U$  is not an exact information-theoretic quantity but a *learned, task-aligned intermediate representation* acting as an inductive bias that facilitates transmission scheduling: the FUE predicted utilities  $u_i^l$  are trained end-to-end to correlate with CP accuracy in a data-driven fashion rather than derived from a closed-form mutual information expression, which is computationally infeasible [4]. The theoretical guarantees in Sec. 3.4 (Theorems 1–2) hold with respect to this learned proxy; their practical value depends on how well  $U$  tracks the true task performance, which we validate empirically in Sec. 4.

**FUE Head.** We implement the FUE as a single  $1 \times 1$  convolution (pointwise linear decoder):  $u_i^l = \text{ReLU}(\mathbf{w}^\top \mathbf{f}_i^l + b)$ , producing a sparse meta utility map  $\mathbf{U}_i \in \mathbb{R}^{1 \times H \times W}$ . Each cell’s receptive field already spans its spatial neighborhood through the encoder’s convolutional layers, so a pointwise head suffices. The FUE is trained end-to-end through the differentiable scheduler (Sec. 3.4): the task loss gradient back-propagates through the scheduling decisions to the FUE weights, aligning higher utility values with higher transmission priority and greater contribution to accuracy.

### 3.4 Transmission Scheduler

Even after transforming the optimization into maximizing the learned utility proxy, the challenges of non-differentiability in scheduling (C2) and the NP-hard combinatorial knapsack problem (C3) still exist. To solve these, we design a scheduling algorithm that is (i) differentiable at training and (ii) deterministic at inference, with a theoretically grounded optimality guarantee under the learned utility proxy for uniform-cost features.

After exchanging meta utility maps  $\{\mathbf{U}_i\}_{i=1}^N$ , the scheduler produces a feature selection mask  $\mathbf{M}_i$  for each agent based on a straightforward and interpretable policy:

1. For each spatial cell  $l$ , select at most one agent with the highest non-zero utility  $\max_j u_j^l$  to transmit.
2. From this set of candidates, greedily admit cells with the highest utility-to-cost ratio until the budget  $B$  is met.

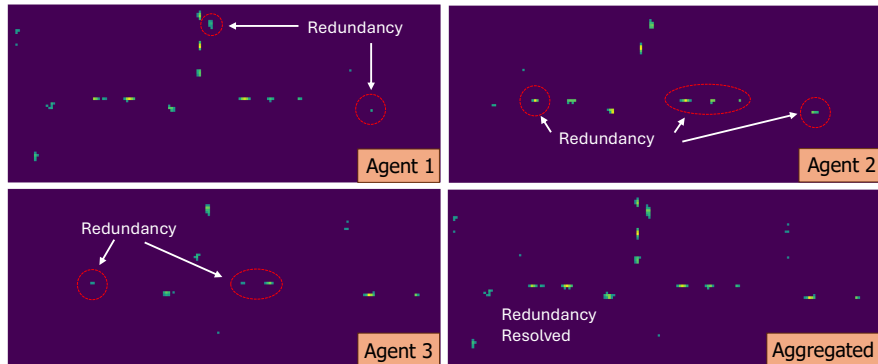


**Fig. 3:** Visualization of meta utility map examples. The top-1 aggregated utility map eliminates redundancy by selecting the agent with the highest utility at each location.

This policy can be deterministically computed by all agents, making it practically compatible with both centralized (V2I) and decentralized (V2V) operation (Sec. 5). We next show that this policy is optimal for the learned utility proxy—*i.e.* it maximizes  $U$  among all feasible schedules, as formalized in Theorem 1 and 2.

**Theorem 1 (Singleton optimality).** *For each cell  $l$ , under the utility proxy in Eq. (4), any maximizer of  $U^l$  selects at most one agent:  $|\{i : m_i^l = 1\}| \leq 1$ .*

*Proof.* Order agents by  $u_1^l \geq u_2^l \geq \dots$ . Selecting agent 1 yields  $U^l = u_1^l$ . Adding agent 2 changes utility by  $u_2^l - \min(u_1^l, u_2^l) = 0$ . Adding any  $k \geq 3$  to a set  $\mathcal{S}$  that already contains agent 1 and 2 yields marginal gain  $u_k^l - \sum_{j \in \mathcal{S}} \min(u_k^l, u_j^l) \leq u_k^l - \min(u_k^l, u_2^l) = 0$ .

Theorem 1 guarantees at most one agent per cell, inherently eliminating cross-agent redundancy (visualized in Fig. 3). This reduces the joint agent-and-cell selection problem (C3) to selecting a subset of cells, each with a single pre-determined agent. Because every cell carries a  $C$ -channel feature vector plus an index, the per-cell cost is uniform for non-zero features [10], and the resulting uniform-cost knapsack is optimally solved by selecting the cells with the largest utilities [13], as formalized in Theorem 2.

**Theorem 2 (Greedy optimality under equal costs).** *Suppose each feature  $(i, l)$  has the same nonzero cost  $C_i^l \equiv c > 0$ . Let the per-frame budget be  $B$  and define the integer capacity  $K \triangleq \lfloor B/c \rfloor$ . Then an optimal solution is obtained by selecting any  $K$  features with the largest utilities  $u_i^l$ .*

We provide the proof to Theorem 2 in Appendix Sec. A. We illustrate the incorporation of the transmission policy into the end-to-end training pipeline below, which is essential in aligning the FUE-learned utility representation with the CP accuracy objective.

**Train-Time Differentiable Scheduling.** Addressing the non-differentiable scheduling challenge (C2), we relax the discrete selection during training. Instead, we model the mask  $m_i^l$  as the composition of two gates:

**(1) Importance gate (scalar, per agent–cell).** We use a logistic gate with temperature  $\eta > 0$ :  $\alpha_i^l = \sigma\left(\frac{u_i^l - \tau}{\eta}\right)$ , where  $\sigma(\cdot)$  is the sigmoid function and  $\tau$  is a learnable threshold. We anneal  $\eta \downarrow 0$  over training to make  $\alpha_i^l$  near-binary.

**(2) Cross-agent top-1 (categorical, per cell).** To model the “pick one agent per cell” constraint differentially, we apply the Gumbel–Softmax reparameterization [12] to the score vector  $\mathbf{u}^l = (u_1^l, \dots, u_N^l)$  with independent Gumbel noise  $g_i^l \sim \text{Gumbel}(0, 1)$  and temperature  $\gamma > 0$ :

$$\beta_i^l(\gamma) = \text{softmax}_i\left(\frac{u_i^l + g_i^l}{\gamma}\right) = \frac{\exp((u_i^l + g_i^l)/\gamma)}{\sum_{k=1}^N \exp((u_k^l + g_k^l)/\gamma)}. \quad (5)$$

We combine these gates using a Straight-Through Estimator (STE) [18]. In the forward pass, we apply the deterministic policy for stability:

$$m_{i\_fwd}^l = \mathbb{I}[u_i^l \geq \tau] \cdot \text{OneHot}\left(i = \arg \max_k u_k^l\right). \quad (6)$$

In the backward pass, we compute gradients as if the mask was the soft, differentiable approximation  $\tilde{m}_i^l = \alpha_i^l \beta_i^l(\gamma)$ .  $\gamma$  follows the same annealing schedule as  $\eta$ .

**Inference-time Deterministic Policy.** At inference, we apply the deterministic policy from the STE’s forward pass. Each agent  $a_i$  applies the thresholding  $\tau$  on the meta utility map  $\mathbf{U}_i$  and exchanges *the sparse meta utility map*, on which the local scheduler applies the per-cell top-1 policy:

$$m_i^l = \mathbb{I}[u_i^l = \max_k u_k^l] \cdot \mathbb{I}[u_i^l \geq \tau]. \quad (7)$$

Let  $C_i^l$  be the cost (bytes) of sending  $\mathbf{f}_i^l$ , and  $\rho_i^l = u_i^l / C_i^l$  the utility–cost ratio. We sort all  $(i, l)$  with  $m_i^l = 1$  by  $\rho_i^l$  and admit the longest prefix whose cumulative cost  $\leq B$ .

**Proposition 1 (Consistency of differentiable and deterministic schedulers).** *For any  $(i, l)$  with  $u_i^l \neq \tau$  and with no injected noise at inference, we have*

$$\lim_{\eta \rightarrow 0^+} \sigma\left(\frac{u_i^l - \tau}{\eta}\right) = \mathbb{I}[u_i^l > \tau], \quad (8)$$

$$\lim_{\gamma \rightarrow 0^+} \beta^l(\gamma) = \text{OneHot}\left(i = \arg \max_k u_k^l\right). \quad (9)$$

Therefore, we have

$$\lim_{\eta \rightarrow 0^+} \tilde{m}_i^l = \mathbb{I}[u_i^l = \max_k u_k^l] \cdot \mathbb{I}[u_i^l > \tau] = m_i^l. \quad (10)$$

Prop. 1 indicates that the train-time policy converges pointwise to the inference policy.

### 3.5 End-to-End Communication-Aware Training

We unify these components into a single end-to-end trainable framework. The final loss combines the downstream task loss (e.g. focal loss) with the semantic loss:

$$\mathcal{L}_{\text{JigsawComm}} = \mathcal{L}_{\text{task}} + \lambda \mathcal{L}_{\text{semantic}}, \quad (11)$$

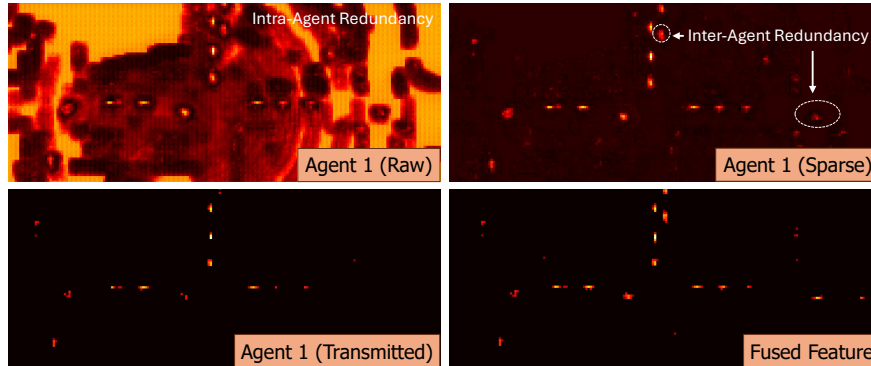


**Fig. 4:** Feature map visualization. The semantic loss and learnable threshold  $\kappa$  produce sparse features that concentrate activations on semantically relevant regions.

where  $\lambda$  balances feature sparsity and task accuracy. The  $\mathcal{L}_{\text{task}}$  gradient flows through the differentiable scheduler (Sec. 3.4) to train the FUE head (Sec. 3.3), while  $\mathcal{L}_{\text{semantic}}$  shapes the encoder (Sec. 3.2). By jointly learning the sparsity threshold  $\kappa$  and utility threshold  $\tau$ , JIGSAWCOMM activates and transmits features only when they contribute to CP accuracy, as illustrated in Fig. 4. We note that a naive alternative—penalizing the transmission masks  $\{M_i\}$  directly—performs worse in practice because it penalizes all communication indiscriminately, disregarding semantic importance and redundancy.

### 3.6 Robustness Enhancement

**Robustness to Misalignment.** The top-1-per-cell policy in Eq. (7) compares utilities  $u_i^l$  across agents at each spatial cell  $l$ . In practice, localization noise and communication delays introduce translational offsets between agents’ coordinate frames [41], causing the scheduler to compare misaligned cells. To address this, we introduce a lightweight alignment step that estimates and corrects offsets using only the already-exchanged meta utility maps  $\{U_i\}$ , requiring no additional communication. Inspired by the feature matching and warping in [40], for each non-ego agent  $j$ , we extract the top- $K$  cells by utility value from both  $U_{\text{ego}}$  and  $U_j$  as sparse keypoint sets and estimate a translational offset  $\delta_j$  via RANSAC [5]: in each iteration, we sample one point from each set, compute the candidate offset, and count inliers within  $\varepsilon$  cells. The best hypothesis is refined by averaging inlier correspondences. Offsets with low confidence are discarded to avoid interpolation artifacts. Given the estimated offsets, each non-ego utility map  $U_j$  and features  $F_j$  are warped by  $\delta_j$  via bilinear grid sampling before scheduling and fusion.

**Robustness to Packet Loss.** The top-1-per-cell policy also provides a natural fallback under packet loss: if a non-ego agent’s scheduled feature is dropped during transmission, the ego vehicle uses its own local feature at the affected cell, requiring no additional communication. Because the ego’s feature is always available and semantically meaningful in visible areas, this fallback degrades gracefully (Appendix E) and guarantees the performance lower-bounded by local detection. Alternatively, a Top- $K$  policy could pre-

**Table 1:** Main results on OPV2V and DAIR-V2X. All methods transmit their full output (unlimited budget  $B$ ). Rel. Eff. is the  $\text{mAP}@0.5$ -to-total-size ratio, normalized to JIGSAWCOMM ( $= 100\%$ ). JIGSAWCOMM achieves SOTA accuracy while reducing data volume by over  $500\times$ .

Method	OPV2V					DAIR-V2X				
	mAP@.5	mAP@.7	Per-Ag.	Total	Rel. Eff.	mAP@.5	mAP@.7	Per-Ag.	Total	Rel. Eff.
			(KB)	(KB)	(%)			(KB)	(KB)	(%)
No Fusion	0.68	0.60	–	–	–	0.50	0.44	–	–	–
F-Cooper [3]	0.89	0.79	8,800	22,792	0.19	0.56	0.39	16,384	32,768	0.70
V2X-ViT [35]	0.87	0.67	8,800	22,792	0.18	0.68	0.50	16,384	32,768	0.84
AttFusion [36]*	0.91	0.82	8,800	22,792	0.19	0.65	0.51	16,384	32,768	0.81
* + Enc-Dec	0.89	0.81	4,400	11,396	0.38	0.65	0.51	8,192	16,384	1.61
Where2comm [10]	0.85	0.60	1,152	2,795	1.47	0.59	0.46	6,295	12,590	1.91
ERMVP [40]	0.89	0.79	845	2,189	1.97	0.64	0.51	2,914	5,827	4.47
CoST [30]	0.87	0.76	4,194	12,163	0.35	0.62	0.47	4,194	8,389	3.01
JIGSAWCOMM	<b>0.92</b>	<b>0.82</b>	<b>17</b>	<b>44</b>	<b>100.00</b>	<b>0.69</b>	<b>0.52</b>	<b>149</b>	<b>282</b>	<b>100.00</b>

select backup agents when more bandwidth is available, where the scheduler pre-selects  $K$  candidate agents per cell and falls back to the next-best candidate upon packet loss.

## 4 Evaluation

### 4.1 Experimental Setup

**Datasets.** We evaluate JIGSAWCOMM on two CP benchmarks: (i) OPV2V [36], a large-scale dataset with 11,464 LiDAR frames from 2–5 agents across 70 scenes in 8 CARLA [6] towns; and (ii) DAIR-V2X [37], the first large-scale real-world CP dataset for vehicle-infrastructure cooperation, containing 71,254 frames.

**Implementation Details.** We adopt PointPillars [16] as the LiDAR BEV backbone and a max-out module as the fusion backbone [3]. We train JIGSAWCOMM for up to 100 epochs using Adam ( $\beta_1 = 0.9, \beta_2 = 0.999$ ), with a base learning rate of 0.002. The Gumbel-Softmax temperatures  $\eta, \gamma$  are annealed from  $0.9 \rightarrow 0.1$ .

**Evaluation Metrics.** We evaluate 3D object detection performance using the mean Average Precision (mAP) at IoU thresholds of 0.5 and 0.7. Communication cost is measured by the Average Total Data Size (KB) transmitted per frame by all agents, under FP8. We also report Relative Communication Efficiency, defined as  $\text{mAP}@0.5/\text{Total Size}$ , normalized to our method (100%) for comparison. The required bandwidth is calculated as the total transmitted feature size multiplied by the frame rate ( $r = 10$  FPS).

**Baselines.** We follow the standard evaluation protocol in communication-efficient CP [11, 21, 33, 43] and evaluate: (i) a *no-fusion* single-vehicle detector; (ii) *full-transmission* intermediate-fusion (F-Cooper [3], V2X-ViT [35], AttFusion [36]); and (iii) *communication-efficient* methods, including the canonical baseline Where2comm [10] and prior art ERMVP (CVPR’24 [40]) and CoST (ICCV’25 [30]). All baselines are reproduced using their official codebases with the PointPillars backbone [16] for a fair comparison.

### 4.2 Quantitative Results

**Main Results.** Table 1 presents our main comparison. On OPV2V, JIGSAWCOMM matches or exceeds all baselines in accuracy, including the best full-transmission method AttFu-

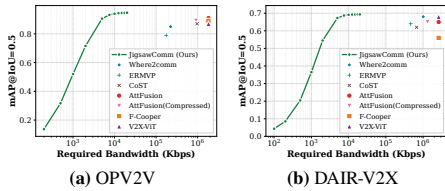


**Fig. 6:** Accuracy vs. required bandwidth. JIGSAWCOMM (curve) is flexible via  $B$ ; baselines (points) are fixed.

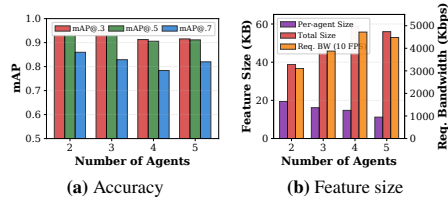


**Fig. 7:** Scalability on OPV2V by #agents. JIGSAWCOMM bounds the payload to  $\mathcal{O}(1)$ .

sion, while using only 44 KB per frame—a  $520\times$  reduction from AttFusion’s 22,792 KB. On the real-world DAIR-V2X dataset, JIGSAWCOMM achieves the highest mAP@0.5 (0.69), surpassing V2X-ViT (0.68) while requiring only 282 KB ( $116\times$  less data). Among communication-efficient baselines, JIGSAWCOMM outperforms the strongest competitor ERMVP by 3 mAP points on OPV2V and 5 on DAIR-V2X, while using  $50\times$  and  $21\times$  less bandwidth, respectively, thanks to the joint encoder–scheduler design eliminating both intra- and inter-agent redundancy simultaneously.

**Accuracy–Bandwidth Tradeoff.** Fig. 6 plots JIGSAWCOMM’s accuracy as a function of the available bandwidth. On OPV2V, JIGSAWCOMM reaches 0.90 mAP@0.5 at only  $\sim 200$  Kbps and saturates beyond  $\sim 1,000$  Kbps, well within the V2X capacity ( $\leq 20$  Mbps) [8, 9]. On DAIR-V2X, the curve saturates at a similarly low bandwidth, confirming that the learned utility proxy successfully identifies the small fraction of features that drive perception accuracy. This property is especially valuable for congested V2X channels, where the scheduler can gracefully degrade by transmitting only the highest-utility cells first. Note that a single trained model serves the entire curve; the budget  $B$  acts as a simple “knob” at inference.

**Scalability with Number of Agents.** Fig. 7 validates  $\mathcal{O}(1)$  data-channel scaling on OPV2V. The total feature size grows only slightly from  $\approx 40$  KB ( $N=2$ ) to  $\approx 58$  KB ( $N=4$ ) due to increased coverage, while accuracy remains high. This sub-linear growth is a direct consequence of the top-1-per-cell policy (Theorem 1): as more agents observe the same region, the scheduler selects only the single best contributor, converting redundancy into bandwidth savings. Note that the OPV2V benchmark groups scenes by the number of participating agents rather than incrementally adding agents to a fixed scene. Consequently, differences in scene composition (object density, spatial layout) across groups can cause slight non-monotonicity in the per-group averages (*e.g.* a small decrease from  $N=4$  to  $N=5$ ). The overall sub-linear trend nevertheless holds clearly across the range. We further test on a custom dataset with 10–20 CAVs (Appendix D): the payload saturates beyond  $\sim 15$  agents, confirming  $\mathcal{O}(1)$  scaling as inter-agent overlap dominates.

**End-to-End Efficiency.** The average end-to-end latency is  $45.82 \pm 26.96$  ms, composed of  $28.27 \pm 23.88$  ms computation on a single RTX 4090 and  $17.55 \pm 7.14$  ms communication at 20 Mbps, which is well within the 100 ms real-time budget for autonomous driving [17]. The meta utility map overhead from all agents is only  $0.08 \pm 0.04$  KB per frame, an average of less than 0.03 KB/agent under FP4.

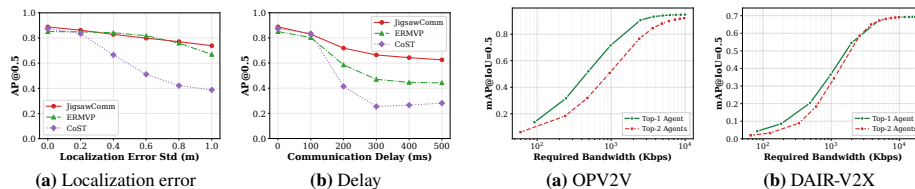


**Fig. 9:** Robustness on OPV2V. JIGSAWCOMM degrades gracefully under localization noise and communication delay.

**Fig. 10:** Top-1 vs. Top-2 agents per cell. Redundant features degrade accuracy, corroborating Theorem 1.

**Table 2:** Ablation study of our core components.

$\mathcal{L}_{sem}$	FUE	OPV2V			DAIR-V2X		
		mAP@0.5	Size (KB)	Rel. Eff. (%)	mAP@0.5	Size (KB)	Rel. Eff. (%)
✓	–	0.93	26,292.4	0.17	0.55	22,670.6	0.99
–	✓	<b>0.94</b>	13,516.8	0.33	0.61	7,375.0	3.38
✓	✓	0.92	<b>43.8</b>	100	<b>0.69</b>	<b>282.0</b>	100

### 4.3 Robustness Analysis

Real-world V2X deployments are subject to imperfect localization and communication delays. We evaluate JIGSAWCOMM’s robustness to both factors on the OPV2V dataset and compare against ERMVP [40] and CoST [30]. We further show JIGSAWCOMM’s robustness against packet drops in Appendix E.

**Localization Error.** We inject Gaussian pose noise with  $\sigma \in \{0, 0.2, \dots, 1.0\}$  m into each agent’s reported position. As shown in Fig. 8a, JIGSAWCOMM degrades gracefully from 0.90 ( $\sigma=0$ ) to 0.74 ( $\sigma=1.0$  m), a relative drop of 18%, thanks to the RANSAC-based utility map alignment (Sec. 3.6). In contrast, CoST drops from 0.87 to 0.39 (55%). The resilience of JIGSAWCOMM stems from the fact that the sparse, high-utility cells used for RANSAC matching are predominantly located on or near objects, providing robust correspondences even under noise. At the practically relevant range of  $\sigma \leq 0.4$  m, JIGSAWCOMM’s accuracy remains above 0.85.

**Communication Delay.** We simulate delays of  $\{0, 100, \dots, 500\}$  ms by substituting each agent’s current features with those from an earlier timestamp. Fig. 8b shows JIGSAWCOMM degrades more gracefully: at 200 ms it retains AP@0.5 of 0.72 (vs. 0.59 ERMVP, 0.41 CoST); at 500 ms—equivalent to 5 missed frames at 10 FPS—JIGSAWCOMM still achieves 0.63, outperforming both baselines by a large margin. We attribute this resilience to two complementary effects: (i) the scheduler selects only the most informative features, so the fused representation is less sensitive to the staleness of any individual contribution; and (ii) the meta utility map and feature warping via RANSAC compensate for spatial misalignment induced by asynchronous transmission [41].

### 4.4 Ablation Study

**Impact of Core Components.** Table 2 ablates  $\mathcal{L}_{semantic}$  and the FUE & Scheduler. Using  $\mathcal{L}_{semantic}$  alone produces sparse features but transmits them in full, yielding 26,292 KB

on OPV2V because inter-agent redundancy is unaddressed. Using the FUE alone selects features intelligently but operates on dense representations (13,517 KB). Only when both are combined does transmission drop to 44 KB while maintaining high accuracy:  $\mathcal{L}_{\text{semantic}}$  ensures each cell carries only task-relevant content (intra-agent), while the scheduler selects only the best contributor per cell (inter-agent). On DAIR-V2X, the synergy is even more pronounced: the full system achieves 0.69 mAP@0.5—substantially higher than either component alone (0.55 or 0.61)—because the real-world dataset’s viewpoint diversity makes both forms of redundancy elimination jointly beneficial.

**Effect of Redundancy.** Theorem 1 predicts that selecting more than the Top-1 agent per cell is suboptimal under our utility proxy. Fig. 10 validates this empirically: a Top-2 policy that transmits features from the two highest-utility agents per cell is worse than Top-1 at nearly every bandwidth point on both datasets. This “more is worse” effect stems from a limitation of current fusion algorithms dominantly adopted by SOTA CP algorithms (*e.g.* max-pooling, attention [3, 10, 36]). *The fused feature can be expressed as a weighted sum of the features from different agents.* If the second-best agent’s feature is noisier or semantically inconsistent, it dilutes the clean, high-utility representation rather than reinforcing it. This corroborates JIGSAWCOMM’s design of selecting only the highest-quality, non-redundant features.

## 5 Discussion

**Practical V2X Deployment.** JIGSAWCOMM maps naturally onto the established dual-channel V2X architecture [8, 9]: meta utility maps on the control channel, sparse BEV features on the data channel via the Collective Perception Message [7]. The scheduler’s utility-ranked priorities integrate directly into both scheduling-based (*e.g.* C-V2X [8]) and contention-based protocols (*e.g.* DSRC [9]), supporting centralized (V2I) and decentralized (V2V) modes for participants in the same communication range.

**Limitations.** The optimality transmission guarantees (Theorems 1–2) hold under the learned utility proxy as a data-driven intermediate representation, not the true task-level objective (which is unavailable during inference for optimizing the transmission decision); their practical value thus depends on how well the proxy tracks perception accuracy (validated empirically in Sec. 4). The current design assumes a shared BEV backbone across agents; heterogeneous architectures would require feature alignment before utility comparison [20]. Finally, the “more is worse” finding (Sec. 4.4) highlights a limitation of existing fusion modules [3, 10, 35, 36]; developing fusion architectures that can leverage multi-agent redundancy synergistically remains an open problem.

## 6 Conclusion and Future Work

**Conclusion.** We present JIGSAWCOMM, a joint semantic feature encoding and transmission framework for cooperative perception that maximizes every transmitted bit’s contribution to the downstream task. By jointly training a sparse semantic encoder and a lightweight Feature Utility Estimator via a differentiable scheduler, JIGSAWCOMM extracts and selects only essential, non-redundant data. The resulting top-1 scheduling policy—optimal under the learned utility proxy—eliminates cross-agent redundancy and bounds the data-channel cost to  $\mathcal{O}(1)$  with respect to the number of agents. Experiments on

OPV2V and DAIR-V2X demonstrate state-of-the-art accuracy with over  $20\text{--}500\times$  bandwidth reduction and strong robustness to localization noise and communication delay.

**Future Work.** Several promising directions remain. First, the sparse features produced by JIGSAWCOMM are amenable to entropy coding, which could further reduce the transmitted payload. Second, extending the framework to joint source-channel coding would enable end-to-end optimization over unreliable wireless channels rather than treating compression and transmission separately. Third, adapting the framework to camera-based BEV features and multi-modal (LiDAR + camera) fusion would broaden its applicability to the heterogeneous sensor suites.

## References

1. Binucci, F., Banelli, P., Di Lorenzo, P., Barbarossa, S.: Adaptive resource optimization for edge inference with goal-oriented communications. *EURASIP Journal on Advances in Signal Processing* **2022**(1) (2022)
2. Chatziioannou, I., Tsigdinos, S., Tzouras, P.G., Nikitas, A., Bakogiannis, E.: Connected and autonomous vehicles and infrastructure needs: Exploring road network changes and policy interventions. In: *Deception in Autonomous Transport Systems: Threats, Impacts and Mitigation Policies*. Springer (2024)
3. Chen, Q., Ma, X., Tang, S., Guo, J., Yang, Q., Fu, S.: F-cooper: feature based cooperative perception for autonomous vehicle edge computing system using 3D point clouds. In: *Proc. of the ACM/IEEE Symposium on Edge Computing (SEC)* (2019)
4. Cover, T.M.: *Elements of information theory*. John Wiley & Sons (1999)
5. Derpanis, K.G.: Overview of the ransac algorithm. *Image Rochester NY* **4**(1), 2–3 (2010)
6. Dosovitskiy, A., Ros, G., Codevilla, F., Lopez, A., Koltun, V.: CARLA: An open urban driving simulator. In: *Proc. of the Conference on Robot Learning (CoRL)* (2017)
7. (ETSI), E.T.S.I.: Intelligent transport system (its); vehicular communications; basic set of applications; collective perception service; release 2 (2023), [https://www.etsi.org/deliver/etsi\\_ts/103300\\_103399/103324/02.01.01\\_60/ts\\_103324v020101p.pdf](https://www.etsi.org/deliver/etsi_ts/103300_103399/103324/02.01.01_60/ts_103324v020101p.pdf), release 2
8. European Telecommunications Standards Institute (ETSI): ETSI EN 303 613 V1.1.1: Intelligent Transport Systems (ITS); Congestion Control Mechanisms for C-V2X PC5 Interface; Access Layer Part (2019), [https://www.etsi.org/deliver/etsi\\_en/303600\\_303699/303613/01.01.01\\_60/en\\_303613v010101p.pdf](https://www.etsi.org/deliver/etsi_en/303600_303699/303613/01.01.01_60/en_303613v010101p.pdf), [Online]
9. Federal Communications Commission (FCC): Dedicated Short Range Communications (DSRC) Service (2025), <https://www.fcc.gov/wireless/bureau-divisions/mobility-division/dedicated-short-range-communications-dsrc-service>, [Online]
10. Hu, Y., Fang, S., Lei, Z., Zhong, Y., Chen, S.: Where2comm: Communication-efficient collaborative perception via spatial confidence maps. *Advances in Neural Information Processing Systems (NeurIPS)* (2022)
11. Hu, Y., Peng, J., Liu, S., Ge, J., Liu, S., Chen, S.: Communication-efficient collaborative perception via information filling with codebook. In: *Proc. of the IEEE/CVF Conference on Computer Vision and Pattern Recognition (CVPR)* (2024)
12. Jang, E., Gu, S., Poole, B.: Categorical reparameterization with gumbel-softmax. *arXiv preprint arXiv:1611.01144* (2016)
13. Kellerer, H., Pferschy, U., Pisinger, D.: Multidimensional knapsack problems. In: *Knapsack problems*, pp. 235–283. Springer (2004)

14. Kim, S.W., Liu, W., Ang, M.H., Frazzoli, E., Rus, D.: The impact of cooperative perception on decision making and planning of autonomous vehicles. *IEEE Intelligent Transportation Systems Magazine* 7(3), 39–50 (2015)
15. Kingma, D.P.: Adam: A method for stochastic optimization. arXiv preprint arXiv:1412.6980 (2014)
16. Lang, A.H., Vora, S., Caesar, H., Zhou, L., Yang, J., Beijbom, O.: Pointpillars: Fast encoders for object detection from point clouds. In: Proc. of the IEEE/CVF Conference on Computer Vision and Pattern Recognition (CVPR) (2019)
17. Lin, S.C., Zhang, Y., Hsu, C.H., Skach, M., Haque, M.E., Tang, L., Mars, J.: The architectural implications of autonomous driving: Constraints and acceleration. In: Proc. of the International Conference on Architectural Support for Programming Languages and Operating Systems (ASPLOS). ACM (2018)
18. Liu, M., Li, Y., Yin, J., Zhang, Z., Yu, C.: Differentiable combinatorial scheduling at scale. In: Proc. of the International Conference on Machine Learning (ICML) (2024)
19. Liu, Y.C., Tian, J., Glaser, N., Kira, Z.: When2com: Multi-agent perception via communication graph grouping. In: Proc. of the IEEE/CVF Conference on Computer Vision and Pattern Recognition (CVPR) (2020)
20. Lu, Y., Hu, Y., Zhong, Y., Wang, D., Chen, S., Wang, Y.: An extensible framework for open heterogeneous collaborative perception. In: The Twelfth International Conference on Learning Representations (2024)
21. Mao, R., Wu, H., Jia, Y., Nan, Z., Sun, Y., Zhou, S., Gündüz, D., Niu, Z.: Diffcp: Ultra-low bit collaborative perception via diffusion model. In: Proc. of the International Conference on Robotics and Automation (ICRA). IEEE (2025)
22. Ng, A.Y.: Feature selection,  $l_1$  vs.  $l_2$  regularization, and rotational invariance. In: Proc. of the International Conference on Machine Learning (ICML) (2004)
23. Pezone, F., Barbarossa, S., Di Lorenzo, P.: Goal-oriented communication for edge learning based on the information bottleneck. In: Proc. of the International Conference on Acoustics, Speech and Signal Processing (ICASSP). IEEE (2022)
24. Qin, Z., Tao, X., Lu, J., Tong, W., Li, G.Y.: Semantic communications: Principles and challenges. arXiv preprint arXiv:2201.01389 (2021)
25. Qiu, H., Huang, P., Asavisanu, N., Liu, X., Psounis, K., Govindan, R.: AutoCast: Scalable infrastructure-less cooperative perception for distributed collaborative driving. In: Proc. of the International Conference on Mobile Systems, Applications, and Services (MobiSys) (2022)
26. Rauch, A., Klanner, F., Raschofer, R., Dietmayer, K.: Car2x-based perception in a high-level fusion architecture for cooperative perception systems. In: Proc. of the IEEE Intelligent Vehicles Symposium (2012)
27. Sheng, Y., Ye, H., Liang, L., Jin, S., Li, G.Y.: Semantic communication for cooperative perception based on importance map. *Journal of the Franklin Institute* 361(6) (2024)
28. Strinati, E.C., Barbarossa, S.: 6G networks: Beyond Shannon towards semantic and goal-oriented communications. *Computer Networks* (2021)
29. Su, W., Chen, L., Bai, Y., Lin, X., Li, G., Qu, Z., Zhou, P.: What makes good collaborative views? contrastive mutual information maximization for multi-agent perception. In: Proc. of the AAAI Conference on Artificial Intelligence (AAAI) (2024)
30. Tang, Z., Liu, Y., Sun, Y., Gao, Y., Chen, J., Xu, R., Liu, S.: CoST: Efficient collaborative perception from unified spatiotemporal perspective. In: Proceedings of the IEEE/CVF International Conference on Computer Vision. pp. 1120–1129 (2025)
31. Wang, R., Cao, G.: Edge-assisted camera selection in vehicular networks. In: Proc. of the IEEE Conference on Computer Communications (INFOCOM) (2024)
32. Wei, Q., Dai, P., Li, W., Liu, B., Wu, X.: Infocom: Kilobyte-scale communication-efficient collaborative perception with information bottleneck. arXiv preprint arXiv:2512.10305 (2025)

33. Xu, J., Zhang, Y., Cai, Z., Huang, D.: CoSDH: Communication-efficient collaborative perception via supply-demand awareness and intermediate-late hybridization. In: Proc. of the IEEE/CVF Conference on Computer Vision and Pattern Recognition (CVPR) (2025)
34. Xu, R., Guo, Y., Han, X., Xia, X., Xiang, H., Ma, J.: Opencda: An open cooperative driving automation framework integrated with co-simulation. In: Proc. of the IEEE International Intelligent Transportation Systems Conference (ITSC) (2021)
35. Xu, R., Xiang, H., Tu, Z., Xia, X., Yang, M.H., Ma, J.: V2X-ViT: Vehicle-to-everything cooperative perception with vision transformer. In: Proc. of the European Conference on Computer Vision (ECCV) (2022)
36. Xu, R., Xiang, H., Xia, X., Han, X., Li, J., Ma, J.: OPV2V: An open benchmark dataset and fusion pipeline for perception with vehicle-to-vehicle communication. In: Proc. of the International Conference on Robotics and Automation (ICRA) (2022)
37. Yu, H., Luo, Y., Shu, M., Huo, Y., Yang, Z., Shi, Y., Guo, Z., Li, H., Hu, X., Yuan, J., et al.: Dair-v2x: A large-scale dataset for vehicle-infrastructure cooperative 3d object detection. In: Proc. of the IEEE/CVF Conference on Computer Vision and Pattern Recognition (CVPR) (2022)
38. Yu, H., Tang, Y., Xie, E., Mao, J., Luo, P., Nie, Z.: Flow-based feature fusion for vehicle-infrastructure cooperative 3d object detection. *Advances in Neural Information Processing Systems (NeurIPS)* (2023)
39. Yuan, Z., Garg, S., Erkip, E., Wang, Y.: Scalable feature compression for edge-assisted object detection over time-varying networks. In: *MLSys Workshop on Resource-Constrained Learning in Wireless Networks* (2023)
40. Zhang, J., Yang, K., Wang, Y., Wang, H., Sun, P., Song, L.: ERMVP: Communication-efficient and collaboration-robust multi-vehicle perception in challenging environments. In: *Proceedings of the IEEE/CVF Conference on Computer Vision and Pattern Recognition (CVPR)*. pp. 12575–12584 (June 2024)
41. Zhang, Q., Zhang, X., Zhu, R., Bai, F., Naserian, M., Mao, Z.M.: Robust real-time multi-vehicle collaboration on asynchronous sensors. In: Proc. of the Annual International Conference on Mobile Computing and Networking (MobiCom) (2023)
42. Zhang, X., Zhang, A., Sun, J., Zhu, X., Guo, Y.E., Qian, F., Mao, Z.M.: Emp: Edge-assisted multi-vehicle perception. In: Proc. of the Annual International Conference on Mobile Computing and Networking (MobiCom) (2021)
43. Zhao, S.Z., Zhang, H., Li, Z., Peng, J., Chui, A., Zhou, Z., Meng, Z., Xiang, H., Huang, Z., Wang, F., et al.: QuantV2X: A fully quantized multi-agent system for cooperative perception. *arXiv preprint arXiv:2509.03704* (2025)
44. Zhou, J., Dai, P., Wei, Q., Liu, B., Wu, X., Wang, J.: Pragmatic heterogeneous collaborative perception via generative communication mechanism. *arXiv preprint arXiv:2510.19618* (2025)

# Supplementary Material

## A Proof to Theorem 2

*Proof.* By Theorem 1, each cell yields at most one admissible candidate; thus the global problem is  $\max_{\mathcal{S} \subseteq \mathcal{C}} \sum_{(i,l) \in \mathcal{S}} u_i^l$  s.t.  $|\mathcal{S}| \leq K$ , where  $\mathcal{C}$  is the set of at-most-one-cell candidates and all costs equal  $c$ . This is a *cardinality-constrained* selection problem. Let  $\mathcal{G}$  be the greedy solution: the  $K$  items with the largest utilities. Assume for contradiction that  $\mathcal{G}$  is not optimal. Let  $\mathcal{O}$  be an optimal solution with  $|\mathcal{O}| \leq K$  and  $\sum_{o \in \mathcal{O}} u(o) > \sum_{g \in \mathcal{G}} u(g)$ . If  $|\mathcal{O}| < K$ , augment  $\mathcal{O}$  by adding the highest-utility items not in  $\mathcal{O}$  until its size reaches  $K$ ; this cannot decrease its objective value because utilities are nonnegative, so w.l.o.g. take  $|\mathcal{O}| = K$ . Order items so that  $u(g_1) \geq \dots \geq u(g_K)$  and  $u(o_1) \geq \dots \geq u(o_K)$ . Since  $\mathcal{G}$  contains the top- $K$  utilities overall,  $u(g_j) \geq u(o_j)$  for every  $j = 1, \dots, K$ . Summing yields  $\sum_j u(g_j) \geq \sum_j u(o_j)$ , a contradiction. Hence  $\mathcal{G}$  is optimal.

## B Architectural Configurations

Given the definitions in Sec. 3, the entire JIGSAWCOMM pipeline can be concisely formulated as follows:

$$\mathbf{z}_i = \text{PillarVFE}(X_i), \quad \mathbf{z}_i \in \mathbb{R}^{P_i \times 64}, \quad \text{for agent } i \quad (1)$$

$$\mathbf{F}_i = \Phi_{\text{enc}}(\text{Scatter}(\mathbf{z}_i)), \quad \mathbf{F}_i \in \mathbb{R}^{C \times H \times W}, \quad (2)$$

$$\mathbf{F}_i \leftarrow \mathbf{F}_i \odot \mathbb{I}[\mathbf{F}_i > \kappa], \quad (3)$$

$$u_i^l = \text{ReLU}(\mathbf{w}^\top \mathbf{f}_i^l + b), \quad \mathbf{U}_i \in \mathbb{R}^{1 \times H \times W}, \quad (4)$$

$$m_i^l = \text{Sched}(\{u_j^l\}_{j=1}^N, \tau, B), \quad \mathbf{M}_i \in \{0, 1\}^{H \times W}, \quad (5)$$

$$\hat{Y} = \Phi_{\text{dec}}(\Phi_{\text{fuse}}(\{\mathbf{M}_i \odot \mathbf{F}_i\}_{i=1}^N)), \quad (6)$$

where  $X_i$  denotes the raw LiDAR point cloud captured by agent  $a_i$ . These points are voxelized and fed into the Pillar VFE [16], yielding  $P_i$  pillar features  $\mathbf{z}_i$  of dimension 64. The pillars are scattered onto a 2D BEV grid of size  $H_0 \times W_0$  and processed by the multi-scale BEV backbone encoder  $\Phi_{\text{enc}}$ , which consists of three downsampling blocks with 3, 5, and 8 convolutional layers at 64, 128, and 256 channels respectively (each with stride-2 entry, BatchNorm, and ReLU), followed by three transposed-convolution upsampling blocks whose outputs are concatenated to produce  $C=384$ -channel features  $\mathbf{F}_i$  at half the input spatial resolution ( $H=H_0/2$ ,  $W=W_0/2$ ).

The sparse thresholding (Eq. 3) zeros out activations below the learnable threshold  $\kappa$ , producing compact features with exact structural sparsity. The FUE head (Eq. 4) is a single  $1 \times 1$  convolution that maps each  $C$ -dimensional feature cell to a scalar utility

**Table 1:** Detailed architectural specifications for JIGSAWCOMM.  $N$  is the number of cooperative agents in a scene,  $P$  the number of non-empty pillars, and  $A$  the number of anchors per cell. With voxel resolution 0.4 m and the default LiDAR range, the initial BEV grid is  $H_0 \times W_0 = 200 \times 704$ ; after the multi-scale backbone the feature map is  $H \times W = 100 \times 352$ .

	Output size	JIGSAWCOMM framework
Pillar VFE	$P \times 64$	Feature augment: cluster & center offsets, 10-d Linear, 64, BN1d, ReLU MaxPool over points
Pillar Scatter	$N \times 64 \times H_0 \times W_0$	Scatter pillar features to BEV grid
BEV Backbone (encoder)	$N \times 256 \times \frac{H_0}{8} \times \frac{W_0}{8}$	Conv3×3, 64, stride 2, BN, ReLU Conv3×3, 64, stride 1, BN, ReLU } × 3 Conv3×3, 128, stride 2, BN, ReLU Conv3×3, 128, stride 1, BN, ReLU } × 5 Conv3×3, 256, stride 2, BN, ReLU Conv3×3, 256, stride 1, BN, ReLU } × 8
BEV Backbone (decoder)	$N \times 384 \times H \times W$	ConvT1×1, 128, stride 1, BN, ReLU ConvT2×2, 128, stride 2, BN, ReLU ConvT4×4, 128, stride 4, BN, ReLU Concat3, 384
Sparse Thresholding	$N \times 384 \times H \times W$	$\mathbf{F}_i \leftarrow \mathbf{F}_i \odot \mathbb{I}[\mathbf{F}_i > \kappa]$ , $\kappa$ learnable
FUE Head	$N \times 1 \times H \times W$	Conv1×1, 1
Transmission Scheduler	$N \times 1 \times H \times W$	Train: $\tilde{m}_i^l = \sigma\left(\frac{u_i^l - \tau}{\eta}\right) \cdot \beta_i^l(\gamma)$ (STE) Infer: $m_i^l = \mathbb{I}[i = \arg \max_k u_k^l] \cdot \mathbb{I}[u_i^l \geq \tau]$ Budget: greedy top- $K$ by $u_i^l$
Fusion	$1 \times 384 \times H \times W$	Element-wise max over $N$ agents
Detection Head	$H \times W \times A$	Cls: Conv1×1, $A$ , stride 1 Reg: Conv1×1, $7A$ , stride 1

$u_i^l$ , forming the meta utility map  $\mathbf{U}_i$ . After exchanging the sparse utility maps among agents, the transmission scheduler (Eq. 5) deterministically computes the binary mask  $\mathbf{M}_i$  via the per-cell top-1 selection, threshold  $\tau$ , and budget constraint  $B$  (Sec. 3.4). The masked features  $\mathbf{M}_i \odot \mathbf{F}_i$  are fused via element-wise max pooling across agents, and the fused representation is passed through two  $1 \times 1$  convolution heads for classification ( $A$  anchors) and bounding-box regression ( $7A$  outputs).

The detailed layer-by-layer specifications are given in Table 1. Notably, JIGSAWCOMM introduces two lightweight additions beyond the standard PointPillar backbone [16]: (i) the FUE head ( $C+1 = 385$  parameters) and (ii) two learnable scalar thresholds  $\kappa$  and  $\tau$ . The transmission scheduler is purely algorithmic with no learnable parameters. The additional parameter overhead is therefore negligible ( $< 0.01\%$  of total model parameters).

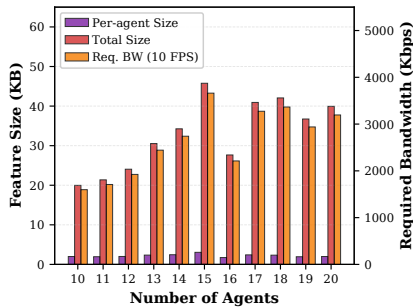


**Fig. 1:** JIGSAWCOMM’s total feature size and required bandwidth under 10 FPS on our custom dataset.

$p_{\text{drop}}$	AP@.3	AP@.5	AP@.7
0.00	0.933	0.925	0.826
0.05	0.930	0.922	0.822
0.10	0.926	0.919	0.817
0.15	0.923	0.915	0.813
0.20	0.919	0.911	0.808

**Table 2:** Robustness to packet loss on OPV2V.  $p_{\text{drop}}$ : per-agent drop probability; ego fallback at affected cells.

## C Training Procedure

**Optimization.** We use Adam [15] with initial learning rate  $2 \times 10^{-3}$ , weight decay  $10^{-4}$ , and  $\epsilon = 10^{-10}$ . The learning rate is decayed by a factor of 0.1 at epochs 15 and 30 using a multi-step schedule. All models are trained for 50 epochs with batch size 4 on a single NVIDIA RTX 4090 GPU. We save checkpoints every 2 epochs and select the model with the lowest validation loss. We select  $\lambda = 1000$  for OPV2V and  $\lambda = 100$  for DAIR-V2X, through standard cross validation.

**Temperature Annealing.** The Gumbel–Softmax temperature  $\gamma$  and importance-gate temperature  $\eta$  share the same annealing schedule: both are initialized to 0.9 and multiplied by a decay factor of 0.9 each epoch, yielding  $\eta_t = 0.9^{t+1}$  at epoch  $t$ . The temperature is clamped at a minimum of 0.01 to maintain numerical stability. As  $\eta \rightarrow 0$ , the differentiable masks converge to the deterministic inference-time policy (Prop. 1).

**Data Augmentation.** During training, we apply three standard augmentations to the global point cloud: (i) random flip along the  $x$ -axis, (ii) random rotation uniformly sampled from  $[-\pi/4, \pi/4]$ , and (iii) random scaling with a factor uniformly sampled from  $[0.95, 1.05]$ .

**Bandwidth Control.** During training, no explicit bandwidth constraint is imposed ( $B = \infty$ ); the semantic loss  $\mathcal{L}_{\text{semantic}}$  and the learnable threshold  $\tau$  naturally drive the model toward compact transmission. At inference, the budget  $B$  can be set to any desired level: the scheduler simply admits cells by descending utility until the budget is met (Sec. 3.4). This allows a single trained model to operate at any point on the bandwidth–accuracy trade-off curve without retraining.

## D Scaling with More Agents

To further test JIGSAWCOMM’s ability to scale beyond the 2-5 agents available from the OPV2V and DAIR-V2X dataset Sec. 4.1, we conducted further experiments on a custom collected dataset. We utilized the CARLA digital driving simulator [6] in conjunction

with the OpenCDA framework [34] for coordinated multi-agent simulation and data recording. The data was collected following the same format and conventions as the public OPV2V benchmark dataset, including sensor configurations, coordinate systems, and CAV parameters, to ensure compatibility with existing CP models and evaluation pipelines. We set up the scene within CARLA’s ‘Town10HD’ map with 10–20 CAVs following realistic traffic rules, at a large multi-lane intersection.

Fig. 1 presents the result of JIGSAWCOMM on the custom dataset. We can observe that JIGSAWCOMM’s total data-channel payload does not double when scaling from 10 to 20 agents. It saturates and remains relatively flat when the number of agents is larger than 15, confirming the asymptotic  $\mathcal{O}(1)$  data-channel scaling. As more agents join, the collective coverage saturates, the overlap becomes dominant, and the marginal contribution of each new agent becomes smaller.

## E Robustness to Packet Loss

In real-world V2X deployments, transmitted feature payloads may be lost due to channel fading, congestion, or collisions at the MAC layer. We study how JIGSAWCOMM behaves when a non-ego agent’s scheduled feature packet is dropped with probability  $p_{\text{drop}} \in \{0, 0.05, 0.10, 0.15, 0.20\}$ .

**Fallback mechanism.** Under the top-1-per-cell policy, each spatial cell is assigned to exactly one agent. When a non-ego agent’s packet is lost, the ego vehicle falls back to its own local feature at the affected cell. Since the ego’s feature is always available (no transmission required), this fallback incurs zero additional communication and requires no retraining. Alternatively, the system can opt for Top- $K$  scheduling when the bandwidth is sufficient.

**Results.** Table 2 reports the results on OPV2V. JIGSAWCOMM exhibits remarkable resilience: even at a 20% packet drop rate, AP@0.5 decreases by only 1.4 percentage points (from 0.925 to 0.911), and AP@0.7 by 1.8 points (from 0.826 to 0.808). The degradation is nearly linear in  $p_{\text{drop}}$ , confirming that there is no catastrophic failure mode. This resilience stems from two properties of JIGSAWCOMM’s design: (i) the top-1 scheduler assigns each cell to the *single highest-utility* agent, so the dropped feature is typically from a non-ego agent that only marginally outperforms the ego’s own observation at that cell (due to less occlusion or high-quality observation); and (ii) the ego’s local feature, while not the top-ranked choice, still provides a semantically meaningful representation for non-occluded objects.

**Top- $K$  as an alternative.** An alternative strategy for handling packet loss, especially for enhancing the detection of occluded objects, is to relax the top-1 policy to a Top- $K$  policy, where the scheduler pre-selects  $K$  candidate agents per cell and falls back to the next-best candidate upon packet loss. However, Top-2 scheduling can incur additional transmission overhead. Therefore, the ego-fallback mechanism is preferable: it achieves the full accuracy benefit of Top-1 scheduling when packets arrive, and gracefully falls back to the ego’s own representation otherwise—all without increasing the nominal bandwidth or requiring changes to the scheduling policy.

## F Qualitative Results

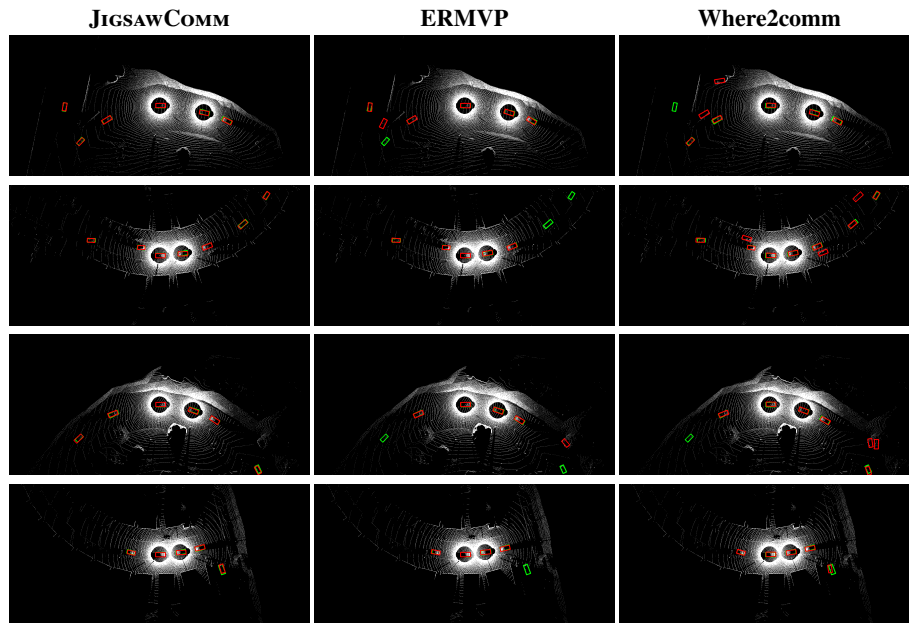


**Fig. 2:** Qualitative comparison of 3D detection results on OPV2V. Each row shows one scene; columns correspond to JigsawComm, ERMVP [40], and Where2comm [10]. **Green:** ground truth; **Red:** predictions. JigsawComm produces tighter bounding boxes with fewer missed detections, especially for distant or partially occluded vehicles.